Journal of Colloid and Interface Science 407 (2013) 546–555

Contents lists available at SciVerse ScienceDirect

Journal of Colloid and Interface Science

www.elsevier.com/locate/jcis

Numerical study of active control of mixing in electro-osmotic flows by temperature difference using lattice Boltzmann methods

A. Alizadeh [a], J.K. Wang [b], S. Pooyan [c], S.A. Mirbozorgi [a], M. Wang [d,e,*]

[a] Department of Mechanical Engineering, University of Birjand, Birjand, Iran
[b] National Institute of Metrology, Beijing 100013, China
[c] Department of Mechanical Engineering, Ferdowsi University of Mashhad, Mashhad, Iran
[d] Department of Engineering Mechanics, Tsinghua University, Beijing 100084, China
[e] Department of Mechanical Engineering, Johns Hopkins University, Baltimore, MD 21214, USA

ARTICLE INFO

Article history:
Received 14 April 2013
Accepted 11 June 2013
Available online 26 June 2013

Keywords:
Electro-osmotic flow
Lattice Boltzmann method
Thermal effects
Active control of mixing

ABSTRACT

In this paper, the effect of temperature difference between inlet flow and walls on the electro-osmotic flow through a two-dimensional microchannel is investigated. The main objective is to study the effect of temperature variations on the distribution of ions and consequently internal electric potential field, electric body force, and velocity fields in an electro-osmotic flow. We assume constant temperature and zeta potential on walls and use the mean temperature of each cross section to characterize the Boltzmann ion distribution across the channel. Based on these assumptions, the multiphysical transports are still able to be described by the classical Poisson–Boltzmann model. In this work, the Navier–Stokes equation for fluid flow, the Poisson–Boltzmann equation for ion distribution, and the energy equation for heat transfer are solved by a couple lattice Boltzmann method. The modeling results indicate that the temperature difference between walls and the inlet solution may lead to two symmetrical vortices at the entrance region of the microchannel which is appropriate for mixing enhancements. The advantage of this phenomenon for active control of mixing in electro-osmotic flow is the manageability of the vortex scale without extra efforts. For instance, the effective domain of this pattern could broaden by the following modulations: decreasing the external electric potential field, decreasing the electric double layer thickness, or increasing the temperature difference between inlet flow and walls. This work may provide a novel strategy for design or optimization of microsystems.

1. Introduction

Induced fluid flow in micro-scale channels, such as those found in "Lab-on-a Chip" devices, is of considerable challenge and interest. Flow generation with mechanical micropumps requires moving parts which complicates the production and control of micropumps. On the other hand, in a rather new method, the fluid is moved by employing the traveling dissolved ions [1]. The efficiency of this non-mechanical method in moving fluids, especially highly viscous fluids, is an important factor justifying the efforts to study this method [2]. The micropumps mentioned above can transfer the fluid easily in a microchannel by applying an external electric field with no need for any mechanical parts. Therefore, the manageability of these micropumps is easier than the mechanical micropumps.

Since the solid–liquid interface can trap electric charges through physical or chemical adsorption [3], a thin layer (about 100 nm thick) is formed near the surface in the liquid side. The net polarity of the charges in this layer is opposite of those in the solid side. The set of this layer and the layer related to the charges on the solid surface is called electric double layer (EDL). Presence of the electric double layer adjacent to the walls of the microchannel can affect the electrolyte flow through the channel and has practical importance.

For instance, if, under the influence of an external electric field, the ions near the walls start to move along the microchannel, the rest of liquid molecules will move with them due to the liquid viscosity. This type of flow is so-called Electro-Osmotic Flow (EOF). The velocity profile of electro-osmotic flows for thin EDLs (in comparison with the microchannel width) is plug like. That is to say, the main part of the velocity profile, relatively far from the walls, is located out of the EDL and, therefore, has no velocity gradient across the channel $\left(\frac{\partial u}{\partial y}=0\right)$. As a result, the shear stress in this region of the flow is zero.

* Corresponding author at: Department of Engineering Mechanics, Tsinghua University, Beijing 100084, China.
E-mail address: moralwang@jhu.edu (M. Wang).

0021-9797/$ - see front matter © 2013 Elsevier Inc. All rights reserved.
http://dx.doi.org/10.1016/j.jcis.2013.06.026

When the electrolyte temperature distribution is uniform, the maximum velocity which is the velocity at the flat part of the velocity profile is obtained using the following equation which is known as Helmholtz–Smoluchowski equation:

$$U_{ref} = -\frac{\varepsilon_0 \varepsilon_r E_x \zeta}{\mu} \quad (1)$$

In this equation, ζ (V) is the walls electric potential and has a negative value, E_x (V/m) is the external electric field strength, ε_0 (C/V m) is the vacuum electric permittivity coefficient, ε_r is the relative electrical permittivity coefficient of the electrolyte, and μ (Pa s) is the dynamic viscosity.

One of the practical advantages of an EOF is the possibility to control this flow by changing the external electric field. For instance, separating different species is easily possible in these flows. Because, the shear velocity which is the effective parameter in separating the species can be easily controlled by changing the external electric field [4]. Polson and Hayes [5] demonstrated the development of external voltage control of EOF for microfabricated fluidic microdevices.

These flows can oscillate with respect to time or space by changing the external electric field and therefore are applicable in changing the mixing processes in microchannels [6]. Wang et al. [7] showed that EOF was able to induce y-directional velocity which enhanced mixing in the microchannels. On the other hand, their results showed that the mixing enhancement is related with the surface zeta potential and the external electric field strength. Obviously, by controlling the effective parameters on the electro-osmotic flow, desired velocity profiles can be obtained. Mirbozorgi et al. [8] numerically showed that non-uniform distribution of the zeta potential on the walls of a microchannel could lead to non-plug velocity profiles. Herr et al. [9], in an experimental investigation, used a microchannel with variable zeta potential on the surfaces and confirmed the idea of production of non-plug profiles. Schasfoort et al. [10] presented a different method to control the velocity field. They changed the amount of zeta potential on the walls and induced accelerating, decelerating, or return flows by varying the external electric field.

One of the secondary but important parameters in controlling the electro-osmotic flow is temperature. Temperature affects this type of flow by changing the ion distribution and physical properties of the liquid. Studies on the convective heat transfer in the microchannels with attitude of increasing the heat transfer and solving the temperature field in the past decade have been considered from temperature view only. For example, Mohiuddin Mala et al. [11] conducted a structural and basic research on temperature distribution in a two-dimensional microchannel. In their research, the Poisson–Boltzmann equation (on the Debye–Huckel approximation) and the momentum equations are analytically solved, while energy equation is numerically solved and the effect of temperature field on the ion distribution and physical properties has been ignored. They showed that with decreasing the EDL thickness, the heat transfer rate will be increased.

Kwak et al. [12] studied the effect of temperature variations on electro-osmotic flow. They used conventional Computational Fluid Dynamics (CFD) methods to solve governing equations. They have considered the EOF in a microchannel with non-uniform wall temperature. In their work, physical properties of fluid are functions of temperature; therefore, the flow field can be affected by temperature field through temperature-dependent physical properties. Their preliminary goal was to control the EOF by manipulating the temperature distribution. They showed that when upper and lower walls of a two-dimensional microchannel have different temperatures, the electro-osmotic flow resembles a shearflow (Couette flow). Besides, if the wall temperatures vary along the channel, a pattern of wavy flow will appear. Zhao et al. [13] mainly tried to find the optimized dimensionless number (κ) with which fluid could be pumped efficiently by electro-osmotic flow. In addition, they studied the effect of Joule heating on the pumping process.

Recently, several studies have been presented in order to model the EOF using the LBM. Most of these studies are used conventional numerical methods to solve the Poisson–Boltzmann equation especially in its 1D linearized form [14–16]. Wang et al. [17] proposed a consistent lattice evolution method which combines a lattice solution for the nonlinear Poisson–Boltzmann equation with lattice solution for the BGK equation for incompressible fluid flows. Chai and Shi [18] analyzed an EOF in a microchannel solving the momentum equation using incompressible lattice Boltzmann method and presented a novel model to solve the Poisson–Boltzmann equation with the lattice Boltzmann method. Shi et al. [19] proposed a straightforward model for relatively thin EDLs $\left(\kappa = Kh = \frac{h}{\lambda} > 200\right)$ in which the value of temperature and velocity at the edge of the EDL is calculated using the dimensional analysis. Then, they omitted the terms related to this layer from momentum and energy equations and used the values obtained by their model on the edge of the EDL as boundary values to solve the rest of flow field. They used lattice Boltzmann method for simple flows with heat transfer to solve momentum and energy equations.

The works mentioned above confirmed that investigation and control of electro-osmotic velocity profile are of great importance. The main objective of the present work is to study the effects of temperature variation on ion distribution along the channel length. These effects are expected to change velocity and internal electric potential fields. In spite of the fact that ion distribution across the channel width might be affected by temperature variations and should be considered, here, we neglect this fact to avoid extra complication. It is observed in the literature that most of the researchers focused on the effects of temperature field on electro-osmotic flow occurring because of variations of temperature related physical properties of fluid in order to control the EOF or analyzing the convection heat transfer in flows with plug like velocity profiles [11–13]. However, it is expected that temperature distribution can change ion distribution and other dynamic characteristics of flow significantly.

It should be noted that for such a case of an EOF, the ion convection should be very slow so that the Boltzmann distribution could maintain; otherwise, the couple PNP + NS model should be solved instead. Wang and Kang [20] presented a framework to solve the dynamic model for electrokinetic flows in microchannels using coupled lattice Boltzmann model. They showed that for a long microchannel with homogenous charged walls, the PB equation is still available for a wide range of EDL thickness. On the other hand, the applicability of the Poisson–Boltzmann model for micro or nanoscale EOF should be considered as a very important theoretical and engineering problem. Wang and Chen [21] showed that: (i) the PB model can still provide good predictions of the ions density profiles up to a very high ionic concentration in the diffusion layer; (ii) The PB model predicts the net charge density accurately as long as the EDL thickness is smaller than the channel width and the predicted electric potential profile is still very accurate up to a very strong EDL interaction.

In the present study, based on which mentioned above, the PB equation is solved with mean temperature for every cross section along the microchannel. This assumption lets us obtain the distribution of ions in the cross sections of channel locally by an exponential Boltzmann distribution equation. Because of a longitudinal variation of temperature in microchannel, the variation in ion distribution along the channel is still possible. The Navier–Stokes, Poisson–Boltzmann, and energy equations are solved simultaneously in an iterative process since they are coupled.

The numerical method for solving the Poisson–Boltzmann and Navier–Stokes equations is based on Wang's model (LPBM) [17]. The energy equation is solved using Wang's model for thermal evolution equation with generalized heat source term [22]. To validate the numerical results, velocity and internal electric potential fields calculated by the code are compared with those yielded by available analytical solutions. In addition, convective heat transfer in a channel is simulated and Nusselt number and local mean temperature values are compared with analytical data.

2. Problem definition

According to Fig. 1, The EOF studied in this paper is an electrolyte flow through a two-dimensional microchannel with length L and width H. The upper and lower plates of the microchannel are kept at temperature T_{wall} and electric potential ζ. The inlet electrolyte is kept at constant temperature T_{in}. We have $T_{in} < T_{wall}$. The fluid motion is caused by the external electric field with strength E_x, applied by use of an Anode and a Cathode placed at the two ends of the microchannel.

The ratio of length to width of this microchannel (L/H) is equal to 5. The electrolyte considered here is symmetric and has 1:1 ionic ratio (it means that the values of ion Valance numbers are equal, $|Z_+| = |Z_-| = Z = 1$). The locations of the anode and cathode plates are selected far enough from the inlet and outlet of the channel, so that the side effects of the inlet and outlet drops are negligible.

In this study, it is assumed that microchannel is made of silicon, and an electrolyte with K^+ and Cl^- ions have been selected as operating fluid. In addition, the zeta potential is assumed to be negative on the fluid-wall interface and its value is in the range of $-100\ \text{mV} \leqslant \zeta \leqslant -25\ \text{mV}$.

The dimensionless parameter κ is defined as $\kappa = KH = \frac{H}{\lambda}$ in which the width of the channel H is non-dimensionalized with the specific thickness of *EDL* (λ):

$$\lambda = K^{-1} = \sqrt{\frac{\varepsilon_0 \varepsilon_r K_B T_{wall}}{2Z^2 e^2 n_{i\infty}}} \tag{2}$$

where T_{wall}, as mentioned in Fig. 1, is the wall temperature used as reference temperature for identifying the thickness of *EDL*. Here, by selecting the value of κ and H, the value of ions concentration, $n_{i\infty}$, is determined. Sometimes, instead of $n_{i\infty}$, the amount of molar concentration, c, is also determined. In such cases, the Molar concentration in kmol/m^3 is calculated as $c = \frac{n_{i\infty}}{1000 N_A}$, where N_A is the Avogadro number. Other physical quantities such as μ, ε_r, and k are only functions of temperature and though constant in a given temperature. The values of these quantities for $T = 19.85\ ^\circ\text{C}$ (=293 K) are presented in Table 1. In this problem with prescription of the values of the H, E_x, ζ Reference velocity is obtained as $U_{ref} = \frac{-\varepsilon_0 \varepsilon_r E_x \zeta}{\mu}$. In this case, the amount of the Reynolds number is defined as $Re = \frac{U_{ref} H}{\nu}$.

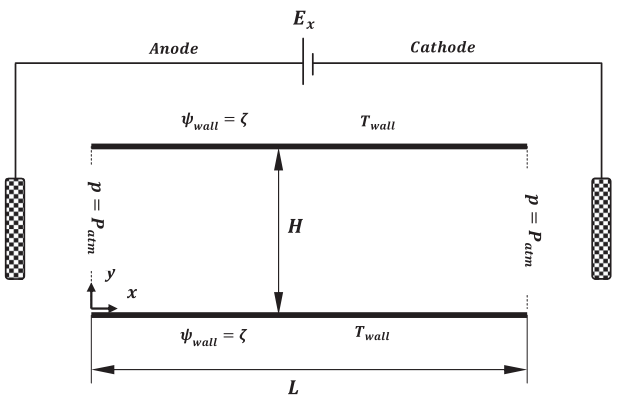

Fig. 1. Schematic of a two-dimensional flat microchannel with constant temperature and zeta potential on the walls.

Table 1
Thermophysical properties and constant parameters at $T = 19.85\ (^\circ\text{C})$ (=293 K).

Variable	Value (Unit)
H	6×10^{-6} m
e	1.602×10^{-19} C
K_B	1.381×10^{-23} J/K
$n_{i\infty}$	6.022×10^{20} ion/m^3
ε_r	80
ε_0	8.854×10^{-12} C/V m
ρ	1000 kg/m^3
μ	1×10^{-3} Pa s
c_p	4180 J /kg K
k	0.613 W/m K

Table 2
Dimensionless parameters and their definitions.

Dimensionless parameters	Definition of the parameters
Pr	$\frac{\nu_{ref}}{\alpha_{ref}}$
Re	$\frac{U_{ref} H_{ref}}{\nu_{ref}}$
A	$\frac{E_{ref} H_{ref}}{\frac{K_B T_{wall}}{Ze}}$
B	$\frac{n_{i\infty} K_B T_{wall}}{\rho_{ref} U_{ref}^2}$
κ	$\sqrt{\frac{2Z^2 e^2 n_{i\infty}}{\varepsilon_0 \varepsilon_r K_B T_{wall}}} H_{ref}$

In the present study for investigating about the effects of temperature difference on the mentioned EOF, the wall temperature is considered constant and here assumed $T_{wall} = 50\ ^\circ\text{C}$. In order to have three amounts of temperature difference between inlet flow and walls of the microchannel, one can consider three inlet flow temperature as: $T_{in} = 12.5\ ^\circ\text{C}$, $T_{in} = 25\ ^\circ\text{C}$, and $T_{in} = 50\ ^\circ\text{C}$.

In summary, for each scenario, the values of c, H, E_x, ζ are determined as the input of problem and then the values of Re and κ are calculated.

Table 2 shows the definitions of the thermal and hydrodynamic dimensionless numbers governing the electro-osmotic flow. In this dimensionless numbers, α (m^2/s) is the thermal penetration coefficient and ν (m^2/s) is the fluid kinematic viscosity. Although the values of variables μ, k, ε_r, and ζ can vary slightly with temperature, in this study, they are considered constant. Their amounts in $T = 19.85\ ^\circ\text{C}$ (=293 K) is used as reference to define the above dimensionless numbers.

While considering Eq. (1), for constant values of E_x and ε_0, the parameters ε_r, μ, and ζ can change with temperature. On the other hand, the zeta potential and permittivity of the pure water are given as [12]: $\varepsilon\ (T) = 2.707 \times 10^{-9}\ \text{C/V m}\ e^{-\frac{T}{219\ \text{K}}}$ and $\zeta\ (T) = -78.2\ \text{mV} - 0.44\ \text{mV/K}\ (T - 273.15\ \text{K})$. Regarding to these relations, this is demonstrated that for temperature range $15\ ^\circ\text{C} < T < 120\ ^\circ\text{C}$, the product $\varepsilon\ (T) \times \zeta\ (T)$ will be approximately constant. As a result, the reference velocity in this temperature range can change only with temperature due to viscosity change as $\frac{1}{\mu(T)}$. In this work, in order to study the effects of temperature variation on ion distribution and consequently the EOF, the viscosity changes with respect to temperature are also ignored. Furthermore, if the external voltage is small, the effect of joule heating (due to electrical resistance of fluid against passing electric charges) on the EOF can be ignored. Because of the low strain rate of the fluid in a wide range of the microchannel width, the viscosity losses are ignored.

3. Continuum formulation

3.1. Poisson–Boltzmann equation

Based on the electrostatic theory [23], the governing equation for the internal electric potential distribution (ψ) can be defined as follows with a Poisson equation:

$$\nabla^2\psi = -\frac{\rho_e(x,y)}{\varepsilon_r\varepsilon_0} \tag{3}$$

where ρ_e is the net electric charge density, $\psi = \psi(x,y)$ is the internal electric potential in 2D space, ε_0 is the vacuum electric permittivity coefficient, and ε_r is the electrolyte electric permittivity ratio $\left(\varepsilon_r = \frac{\varepsilon}{\varepsilon_0}\right)$. The net electric charge density ρ_e can be defined as:

$$\rho_e = Ze(n^+ - n^-) \tag{4}$$

where n^+ and n^- are the numerical concentrations of the positive and negative ions in ion/m^3, respectively. Z is the ions valance number and e is the electric charge of an electron in Cullen C. According to the electrostatic theory, the ion concentration also depends on the internal electric potential distribution ψ. In other words, internal electric potential distribution is a result of a balance between the forces due to ions distribution and electric potential gradient. For instance, in one dimensional case:

$$K_BT\left(\frac{dn^\pm}{dy}\right) = \mp Zen^\pm\left(\frac{d\psi}{dy}\right) \tag{5}$$

In Eq. (5), the left and right sides introduce the ion distribution force and the internal electric potential gradient force, respectively. $n^\pm$ represents the concentration of the positive and negative ions. T is the absolute temperature in Kelvin (K) and K_B is the Boltzmann constant in J/K.

When we assume that $T = T_{mean}(x) = \left(\frac{1}{A(x)}\right)\int TdA$ and if the ions concentration for $\psi = 0$ is $n_{i\infty}$, then integration of Eq. (5) is available and defined as:

$$n^\pm = n_{i\infty}e^{\mp\frac{Ze\psi(x,y)}{K_BT_{mean}(x)}} \tag{6}$$

Eq. (6) is known as the Boltzmann ion distribution equation. In addition to the method mentioned above, Eq. (6) can be proved using statistical thermodynamic concepts. In Eq. (6), the concentration distribution of positive ions is denoted with n^+ and that of negative ions is denoted with n^-. Two important points should be considered here. First, the Nernst–Planck is the main equation governing the ion distribution. Second, while deriving the Boltzmann ion distribution equation from the Nernst–Planck equation, if T is not considered constant in the y direction, taking the integral of Eq. (5) and obtaining the Boltzmann ion distribution equation is not possible. If we cannot derive the Boltzmann ion distribution equation from Nernst–Planck equation, it is not possible to use the Boltzmann ion distribution equation to find the ions distribution in the y direction which is perpendicular to the microchannel walls. This is the reason for considering the $T_{mean}(x)$ in Eq. (6) in the present study.

Combining Eq. (4) and Eq. (6), the net electric charge density equation is obtained as follows:

$$\rho_e(x,y) = -2Zen_{i\infty}\sinh\left(\frac{Ze\psi(x,y)}{K_BT_{mean}(x)}\right) \tag{7}$$

Also, the Poisson–Boltzmann equation is obtained by the combination of Eq. (3) and Eq. (7):

$$\nabla^2\psi = \frac{2Zen_{i\infty}}{\varepsilon_0\varepsilon_r}\sinh\left(\frac{Ze\psi(x,y)}{K_BT_{mean}(x)}\right) \tag{8}$$

where e (C) is the absolute charge of the electron and T_{mean} (K) is the mean temperature at each cross section of the microchannel. Defining appropriate references as below, the non-dimensional form of Eq. (8) is introduced as:

$$\bar\psi = \frac{\psi}{\frac{K_BT_{wall}}{Ze}},\quad \bar\rho_e = \frac{\rho_e}{Zen_{i\infty}},\quad \bar x = \frac{x}{H},\quad \bar y = \frac{y}{H}$$
$$\frac{\partial^2\bar\psi}{\partial\bar x^2} + \frac{\partial^2\bar\psi}{\partial\bar y^2} = -\frac{\kappa^2\bar\rho_e}{2} \tag{9}$$

Boundary conditions governing Eq. (9) are:

$$y = 0 \to \psi = \zeta,\quad y = H \to \psi = \zeta$$
$$x = 0 \to \psi = 0,\quad x = l \to \frac{\partial\psi}{\partial x} = 0 \tag{10}$$

3.2. Modified Navier–Stokes equations

In this study, the modified Navier–Stokes equations are considered based on the electric body force. This body force is due to the application of the external electric field on the net electric charge density available in the *EDL* near the walls. Therefore, the modified Navier–Stokes equations including continuity and momentum equations for incompressible electrolyte flow in laminar steady state are expressed as follows [8]:

$$\text{(a)}\ \nabla\cdot\boldsymbol{u} = 0$$
$$\text{(b)}\ \rho(\boldsymbol{u}\cdot\nabla\boldsymbol{u}) = -\nabla p + \mu\nabla^2\boldsymbol{u} - \rho_e(\boldsymbol{E} + \nabla\psi) \tag{11}$$

where $\boldsymbol{u}$ is the velocity vector in m/s, μ (Pa s) is the dynamic viscosity of the electrolyte (here, independent of temperature), $\boldsymbol{E}$ (V/m) is the external electric field intensity vector, ρ (kg/m^3) is the density of the electrolyte (here, independent of temperature), and p (Pa) is the hydrodynamic pressure of the fluid. The last term in the right hand side of Eq. (11b) represents the electrical body force applied to the fluid and it is the cause of fluid motion. Hereinafter, the body force in the x direction (shown with *BF* and called electric body force in this paper) is defined as:

$$BF = \rho_e\left(E_x - \frac{\partial\psi}{\partial x}\right) \tag{12}$$

It is noteworthy that in this study, no pressure gradient is applied in the direction of the main flow. Since $E_y = 0$ and also due to low concentration of the ions dissolved in the fluid, the term representing the body force in y direction in Eq. (11b) is eliminated [24]. In other words, the electrical force due to the gradient of ψ in the y direction is balanced with the force due to ions distribution. As a result, the Boltzmann ion distribution is obtained.

Balancing these two forces is justified only for ions. Because of low ion concentration in the electrolyte, less number of fluid molecules will be affected by the ion movement. In a similar case, for body force equation (Eq. (12)), $\frac{\partial\psi}{\partial x}$ has an external source and therefore is added to E_x. It is worth noting that the force due to $\frac{\partial\psi}{\partial x}$ has not been balanced with any other forces, unlike the force resulting from $\frac{\partial\psi}{\partial y}$ which is balanced with the forces due to ions distribution.

The dimensionless form of the momentum equations are as follows:

$$\bar u = \frac{u}{U_{ref}},\quad \bar v = \frac{v}{U_{ref}},\quad \bar p = \frac{P}{\rho U_{ref}^2},\quad A = \frac{E_{ref}H}{\frac{K_BT_{wall}}{Ze}},\quad B = \frac{n_{i\infty}K_BT_{wall}}{\rho U_{ref}^2}$$
$$(\bar{\boldsymbol{u}}\cdot\bar\nabla\bar{\boldsymbol{u}}) = -\bar\nabla\bar p + \frac{1}{Re}\bar\nabla^2\bar{\boldsymbol{u}} + \bar\rho_eB(A\bar{\boldsymbol{E}} - \bar\nabla\bar\psi) \tag{13}$$

Boundary conditions governing the Navier–Stokes equations are as follows:

$$y=0\rightarrow u=v=0,\quad y=H\rightarrow u=v=0$$
$$x=0\rightarrow \frac{\partial u}{\partial x}=\frac{\partial v}{\partial x}=0,\quad p=P_{atm} \tag{14}$$
$$x=l\rightarrow \frac{\partial u}{\partial x}=v=0,\quad p=P_{atm}$$

3.3. Energy equation

Regarding all the assumptions expressed in Section 2, the energy equation is defined as follows without any heat source.

$$\rho c_p(\boldsymbol{u}\cdot\nabla T)=k\nabla^2 T \tag{15}$$

where c_p (J/kg K) is the specific heat capacity and k (W/m K) is the fluid thermal conductivity. Using the definition of the dimensionless temperature ($\overline{T}=\frac{T-T_{wall}}{T_{mean}-T_{wall}}$) and considering the dimensionless lengths [$\bar{x},\bar{y}$] and dimensionless velocities [$\bar{u},\bar{v}$] introduced in Eqs. (9) and (13), the energy equation is obtained as:

$$(\bar{\boldsymbol{u}}\cdot\overline{\nabla T})=\frac{1}{Re\times Pr}\overline{\nabla^2 T} \tag{16}$$

Boundary conditions governing the energy equation are:

$$y=0\rightarrow T=T_0,\quad y=H\rightarrow T=T_0$$
$$x=0\rightarrow T=T_{in},\quad x=l\rightarrow \frac{\partial T}{\partial x}=0 \tag{17}$$

Hereinafter, the dimensionless parameters will be shown without (–) sign over them.

4. Lattice Boltzmann models

In the present paper, three governing equations (Navier–Stokes, Poisson–Boltzmann and energy) which are governing the phenomenon under study are solved numerically using the lattice Boltzmann method. Therefore, it is necessary to introduce the equivalent equations used in the lattice Boltzmann method.

4.1. Lattice Poisson–Boltzmann method

4.1.1. Lattice Boltzmann method for fluid with external forces

This section presented two methods in order to implement the external forces in the lattice Boltzmann method. The first method is based on a model presented by Wang et al. [17] in which the external force term is introduced directly into the evolution equation as a distribution function. This method could be named as the method of external force distribution function. The second method is based on modifying the velocity field by the amounts of external forces before computing the equilibrium distribution function.

4.1.1.1. External force distribution function method. The discrete Boltzmann density distribution equation for solving the Navier–Stokes equations in the presence of external forces is indicated as follows:

$$f_i(\boldsymbol{X}+e_i\delta_t,\quad t+\delta_t)-f_i(\boldsymbol{X},t)=-\frac{1}{\tau_f}[f_i(\boldsymbol{X},t)-f_i^{eq}(\boldsymbol{X},t)]+\delta_t F_i \tag{18}$$

where index i is assigned values from 0 to 8 in the standard $D2Q9$ lattice. f_i is the density distribution function at the place $\boldsymbol{X}$ and time t. v is the kinematic viscosity which is related to the relaxation time τ_f as $v=(\tau_f-0.5)C_s^2\delta_t$. C_s is the speed of sound in the fluid having relation with the speed of particles in the lattice $c=\frac{\delta_x}{\delta_t}$ as $C_s=\frac{c}{\sqrt{3}}$. F_i is the external force distribution function at the same time and place and defined as follows:

$$F_i=\frac{(-\nabla p+\rho_e\boldsymbol{E}-\rho_e\nabla\phi)\cdot(\boldsymbol{e_i}-\boldsymbol{u})}{RT}f_i^{eq} \tag{19}$$

where p is the pressure, ϕ is the stream electrical potential caused by the ion movements in the solution based on the Nernst–Planck theory, and $\boldsymbol{E}$ is the electrical field strength.

The Maxwell–Boltzmann equilibrium distribution function for Eqs. (18) and (19) is:

$$f_i^{eq}=\left(e^{-\frac{\varphi}{K_BT}}\right)\left(\omega_i\rho\left[1+\frac{3(\boldsymbol{e_i}\cdot\boldsymbol{u})}{c^2}+\frac{9(\boldsymbol{e_i}\cdot\boldsymbol{u})^2}{c^4}-\frac{3}{2}\frac{(\boldsymbol{u}\cdot\boldsymbol{u})}{c^2}\right]\right) \tag{20}$$

where φ is the potential energy of the conservative force field, $\boldsymbol{u}$ is the macroscopic velocity vector and ρ is the density of the fluid. ω_i is presented the weighting factors for $D2Q9$ lattice as follows:

$$\omega_i=\frac{4}{9}\quad i=0$$
$$\omega_i=\frac{1}{9}\quad i=1,2,3,4 \tag{21}$$
$$\omega_i=\frac{1}{36}\quad i=5,6,7,8$$

4.1.1.2. Modifying velocity method. In this method, the discrete Boltzmann distribution function is defined as the conventional format as follows:

$$f_i(\boldsymbol{X}+\boldsymbol{e_i}\delta_t,t+\delta_t)-f_i(\boldsymbol{X},t)=-\frac{1}{\tau_f}[f_i(\boldsymbol{X},t)-f_i^{eq}(\boldsymbol{X},t)] \tag{22}$$

The equilibrium distribution function is defined as:

$$f_i^{eq}=\omega_i\rho\left[1+3(\boldsymbol{e_i}\cdot\boldsymbol{u})+\frac{9}{2}(\boldsymbol{e_i}\cdot\boldsymbol{u})^2-\frac{3}{2}\boldsymbol{u}\cdot\boldsymbol{u}\right] \tag{23}$$

The fluid can be moved by either the boundaries or the body force. If the body force is the driving force for the fluid flow, the velocity can be modified before computing the equilibrium distribution function (Eq. (23)) as follows [25]:

$$\boldsymbol{F}=m\boldsymbol{a}=\frac{m d\boldsymbol{u}}{dt}\rightarrow\Delta\boldsymbol{u}=\frac{(\tau_f\delta_t)\boldsymbol{F}}{\rho}=\frac{\tau_f\boldsymbol{F}}{\rho} \tag{24}$$

According to assumptions mentioned in Section 3.2 for body force in EOF (Eq. (12)), Eq. (24) can be rewritten as:

$$u_{new}(x,y)=u_{old}(x,y)+\frac{\tau_f}{\rho}\left(g_{rhs}(x,y)\varepsilon_r\varepsilon_0\left(E_x-\frac{\partial\psi}{\partial x}\right)\right) \tag{25}$$

where the right hand side (rhs) of Eq. (8) is defined as $g_{rhs}(x,y)=-\frac{2Zen_{i\infty}}{\varepsilon_0\varepsilon_r}\sinh(\frac{Ze\psi(x,y)}{K_BT_{mean}(x)})$.

The macroscopic values of the density, velocity, and pressure are calculated for both methods mentioned above as follows:

$$\rho=\sum_{i=0}^{8}f_i,\quad \rho u=\sum_{i=0}^{8}f_i e_i,\quad p=C_s^2\rho=\frac{\rho}{3} \tag{26}$$

4.1.2. The lattice Poisson method for solving the Poisson–Boltzmann equation

The evolution equation for the electrical potential on the 2D discrete lattices according to the Wang model is written as follows [17]:

$$g_i(\mathbf{X}+\boldsymbol{e_i}\delta_{t,g},t+\delta_{t,g})-g_i(\mathbf{X},t)=-\frac{1}{\tau_g}\left[g_i(\mathbf{X},t)-g_i^{eq}(\mathbf{X},t)\right]+\left(1-\frac{0.5}{\tau_g}\right)\delta_{t,g}\omega_i g_{rhs} \tag{27}$$

where g_i is the electric potential distribution function, $\boldsymbol{X}$ is the place vector, $\boldsymbol{e_i}$ is the microscopic velocity vector of the particles in nine directions, $\delta_{t,g}$ is the time step, and here, it is equal to 1. τ_g is the dimensionless relaxation time which is defined as:

$$\tau_g = \frac{3\chi\delta_{t,g}}{2\delta_x^2} + 0.5 \tag{28}$$

where δ_x is the lattice constant and χ is the electric potential diffusivity coefficient which is equal to unity in this simulation. g_i^{eq} is the Maxwell–Boltzmann equilibrium distribution function for electric potential. The Maxwell–Boltzmann distribution function for Poisson–Boltzmann equation is:

$$g_i^{eq}(X,t) = \varpi_i \psi \tag{29}$$

where ϖ_i is the weight factor:

$$\varpi_i = \begin{Bmatrix} 0 & i=0 \\ \frac{1}{6} & i=1,2,3,4 \\ \frac{1}{12} & i=5,6,7,8 \end{Bmatrix} \tag{30}$$

Finally, the macroscopic amount of the electric potential is calculated as:

$$\psi = \sum_{i=0}^{8}(g_i + 0.5\delta_{t,g}\omega_i g_{rhs}) \tag{31}$$

4.2. Lattice Boltzmann model to solve the energy equation

In order to obtain the energy equation in lattice Boltzmann method, Boltzmann equation is written based on the internal energy and the internal energy distribution function is defined. As a result, the Boltzmann energy equation which is equivalent to energy equation in continuum space will be obtained. Wang et al. [22] presented a thermal evolution equation based on the internal energy equation with generalized heat source term, which can involve viscous dissipation, pressure compression, and any external heat source. According to assumptions mentioned in Section 2, in the present study, internal heat sources such as Joule heating and viscous dissipation are negligible ($\dot{Q}=0$). Therefore, whatever we have liquid or solid the evolution equation can be generally given as [22]:

$$\theta_i(\boldsymbol{X}+\boldsymbol{e_i}\delta_t, t+\delta_t) - \theta_i(\boldsymbol{X},t) = -\frac{1}{\tau_\theta}[\theta_i(\boldsymbol{X},t) - \theta_i^{eq}(\boldsymbol{X},t)] + \omega_i\left(1-\frac{0.5}{\tau_\theta}\right)\left(\frac{\dot{Q}}{\rho c_p}\right) \tag{32}$$

where θ_i is the internal energy distribution function and τ_θ is the dimensionless relaxation time as $\tau_\theta = \frac{3}{2}\frac{\alpha}{c^2\delta_t} + 0.5$. Clearly, $\dot{Q}$ is the heat source term in the problem. The Maxwell–Boltzmann equilibrium function for Eq. (32) is as follows [22]:

$$\begin{aligned}
\theta_i^{eq} &= -\bar{\vartheta}_i T\frac{\boldsymbol{u}\cdot\boldsymbol{u}}{C^2} \quad i=0 \\
\theta_i^{eq} &= \bar{\vartheta}_i T\left[\frac{3}{2}+\frac{3\boldsymbol{e_i}\cdot\boldsymbol{u}}{2c^2}+\frac{9(\boldsymbol{e_i}\cdot\boldsymbol{u})^2}{2c^4}-\frac{3\boldsymbol{u}\cdot\boldsymbol{u}}{2c^2}\right] \quad i=1,2,3,4 \\
\theta_i^{eq} &= \bar{\vartheta}_i T\left[3+\frac{3\boldsymbol{e_i}\cdot\boldsymbol{u}}{c^2}+\frac{9(\boldsymbol{e_i}\cdot\boldsymbol{u})^2}{2c^4}-\frac{3\boldsymbol{u}\cdot\boldsymbol{u}}{2c^2}\right] \quad i=5,6,7,8
\end{aligned} \tag{33}$$

with

$$\bar{\vartheta}_i = \begin{Bmatrix} -\frac{2}{3} & i=0 \\ \frac{1}{9} & i=1,2,3,4 \\ \frac{1}{36} & i=5,6,7,8 \end{Bmatrix} \tag{34}$$

where T is the temperature of the fluid. The macroscopic value of the temperature is calculated as follows:

$$T = \sum_{i=0}^{i=8}\theta_i + \frac{\delta_t}{2}\frac{\dot{Q}}{\rho c_p} \tag{35}$$

4.3. Boundary conditions in the lattice Boltzmann method

Considering the boundary conditions mentioned in Section 3 for Navier–Stokes, Poisson–Boltzmann and energy equations, it is necessary to impose these boundary conditions on the lattice Boltzmann method equations too. The Zou and He method [26] to impose the velocity boundary conditions, Wang et al. method [17] for internal electric potential boundary conditions and Liu et al. method [27] for the energy equation boundary conditions, are used.

5. Results and discussion

In this section, a numerical solution of an isothermal EOF and simple convection heat transfer in a channel are validated with available analytical solutions. Then, an EOF in a flat microchannel under the effect of the temperature field is studied.

5.1. Benchmarks

If the isothermal EOF scenario in the microchannel defined in Section 2 is fully developed hydrodynamically and ionically, since the relation $\frac{Ze\zeta}{K_B T} \leqslant 1$ is valid, the Debye–Huckel approximation can be used and as a result an analytical solution for velocity and internal electric potential can be obtained as follows [24]:

$$\begin{aligned}
&\text{(a)}\ \frac{\psi}{\zeta} = \frac{\cosh\left(\kappa y - \frac{\kappa H}{2}\right)}{\cosh\left(\frac{\kappa H}{2}\right)} \\
&\text{(b)}\ \left[1-\frac{u}{U_{ref}}\right] = \frac{\cosh\left(\kappa y - \frac{\kappa H}{2}\right)}{\cosh\left(\frac{\kappa H}{2}\right)}
\end{aligned} \tag{36}$$

For numerical solution of the problem, a lattice with 501×101 nodes is selected. Two values of 6.32 and 19.7 are considered for the parameter κ to express the ratio of the EDL thickness to the microchannel width. For both values of κ, the Reynolds number is chosen equal to 5.319×10^{-5}.

Fig. 2 shows the comparison between lattice Boltzmann method and analytical solution results for internal electric potential and velocity field. The close agreement observed between the analytical results and simulations validates the numerical model developed in this study and its underlying assumptions.

To validate the results of energy equation solution with lattice Boltzmann method, a hydrodynamically developed flow driven by body force in a channel of $\frac{L}{H}=20$ is considered. The temperature of the channel walls, T_{wall}, and also the inlet electrolyte temperature, T_{in}, are assumed constant and $T_{in} < T_{wall}$. With $Re = 82.08$ and $Pr = 0.7842$, the analytical solutions for local Nusselt number and local mean temperature along the length of the channel are functions of the Gratz dimensionless number ($x^+ = \frac{\frac{x}{H}}{Re\times Pr}$). These solutions are available in the literature based on the infinite series [28].

Fig. 3 shows the results of Lattice Boltzmann method solution and analytical solution for local Nusselt number and local mean temperature. The figure demonstrates the good accordance between the lattice Boltzmann results and the analytical solution in fully developed region. Results illustrated in Fig. 3 show that the values calculated by lattice Boltzmann method have some difference comparing with to analytical solution in developing flow region. The minor discrepancy between the numerical results and analytical solution is due to the relatively low accuracy of the infinite series results when $Pe = Re \times Pr < 100$ considering that in this case study $Pe = 64.36$.

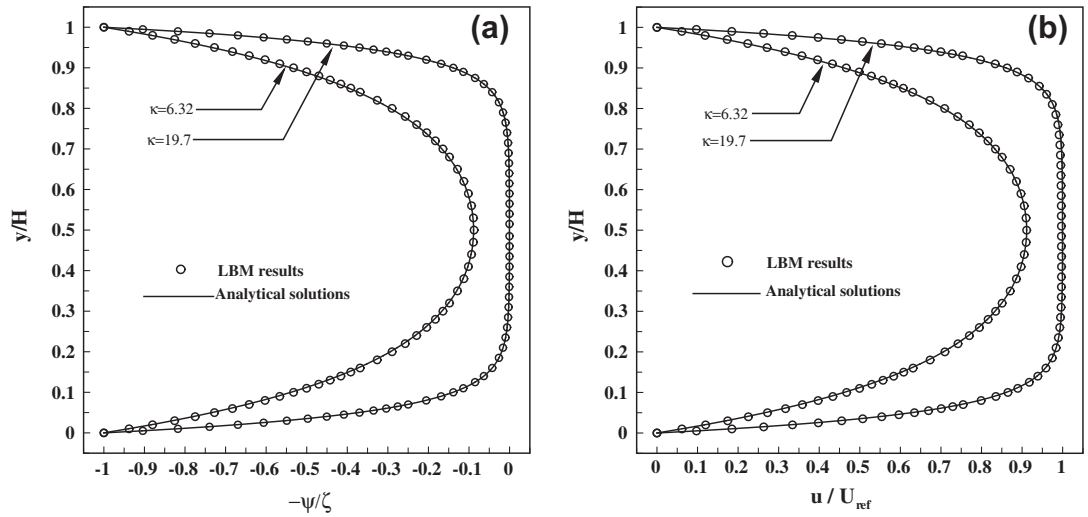

Fig. 2. Comparison between the analytical solution [24] and Lattice Boltzmann method for ideal EOF with $E_x = 500$ V/m and $\zeta = -25$ (mV). (a) Internal electric potential distribution. (b) Velocity Profile.

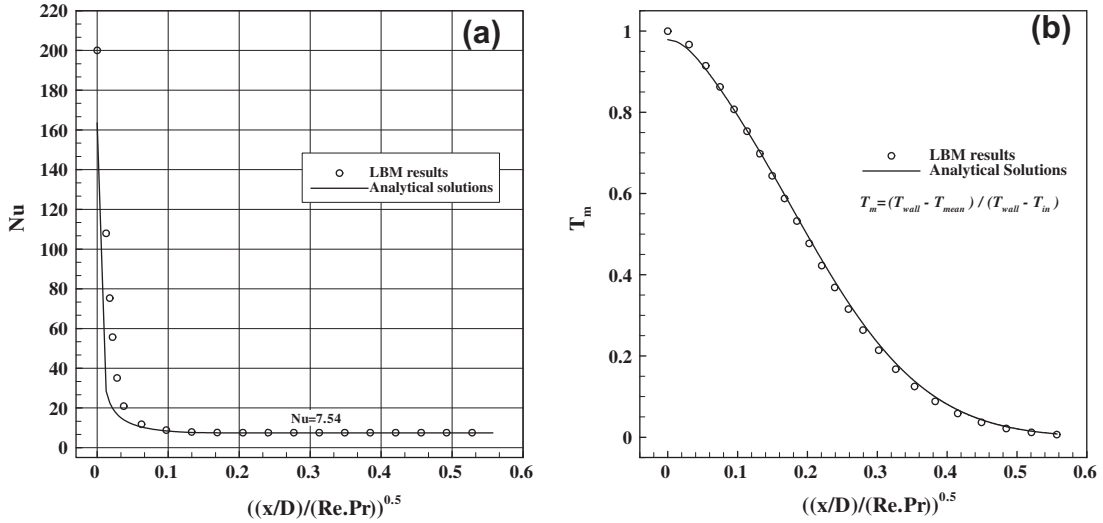

Fig. 3. Comparison between the analytical solution [28] and the LBM results for $Re = 82.08$ and $Pr = 0.7842$. (a) Local Nusselt number. (b) Local mean temperature.

5.2. Temperature difference effects on the EOF

In this part, the temperature effects on the EOF will be discussed. One can non-dimensionalized the temperature difference between walls and inlet electrolyte by dividing it to the wall temperature. Therefore, the dimensionless temperature difference is introduced as $\Delta T = \frac{T_{wall}-T_{in}}{T_{wall}}$. Regarding to those mentioned in Section 2, we have three temperature differences as $\Delta T = 0.0$, $\Delta T = 0.5$ and $\Delta T = 0.75$.

Fig. 4 shows streamlines of the electro-osmotic flow (solid lines) and lines of constant internal electric potential (dotted lines). Fig. 4a shows the EOF considering an isothermal scenario ($\Delta T = 0.0$). It is worth mentioning that since there is no temperature gradient, we have $\left|\frac{\partial \psi}{\partial x}\right| = 0$ for entire channel. Namely, constant internal electric potential lines will be horizontal along the channel.

Fig. 4b and c shows that when ΔT increases (with constant E_x and κ), a pattern of return flow with symmetrical vortices relative to the center line of the microchannel is generated. For both of the two temperature differences, the streamlines at the first zone of the microchannel (at the temperature developing zone) gradually tend toward the center line. It is observed that by increasing the ΔT, at each cross section, $\left|\frac{\partial \psi}{\partial y}\right|$ near the walls gets larger. Therefore, we have sharper internal electric potential gradients near the walls.

Comparison between Fig. 4c and d shows that by increasing κ (with constant E_x and ΔT) the return flow zone at the beginning of the channel grows larger and therefore more volume of fluid is affected by the return flow pattern mentioned above. Comparing Fig. 4d and e it is observed that, increasing the E_x prevents from formation of any return flow at the entrance of the microchannel. However, the streamlines at the beginning of the microchannel in Fig. 4e are more inclined toward the center than Fig. 4b. Fig. 4f demonstrates that despite applying higher external electric field, the effects of ΔT on the electro-osmotic flow is not completely disappeared and $\psi = cte$ lines and streamlines have small inclination toward the center of the microchannel.

For cases with $\Delta T \neq 0$ in Fig. 4, it is observed that far enough from the inlet of the microchannel, the streamlines and constant internal electric potential lines are totally horizontal along the length of the channel (it means that: $\left|\frac{\partial u}{\partial x}\right| = \left|\frac{\partial \psi}{\partial x}\right| = 0$). The reason for this effect is the absence of temperature variations along the

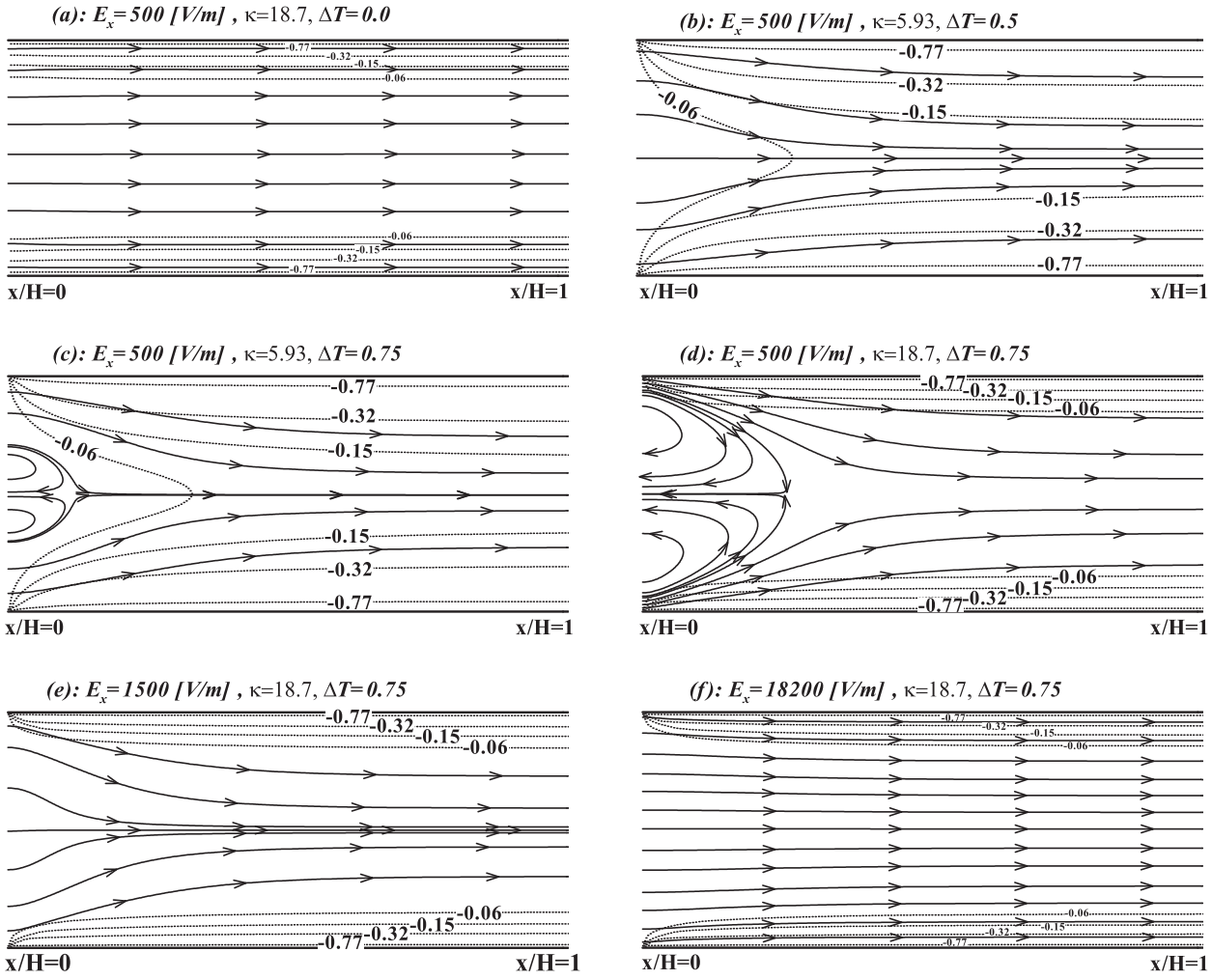

Fig. 4. Streamlines (solid lines) and constant internal electric potential lines (dotted lines) for EOF with different E_x, κ and ΔT.

length of the channel in the mentioned region. Namely, where the temperature difference between the walls and the electrolyte approaches zero, the "mean temperature" variation along the length approaches zero and we have $\frac{\partial T_{mean}}{\partial x} = 0$. Fig. 4a demonstrated the validity of this reason.

According to the results of this section, the most significant effect of the non-isothermal flow field on the electro-osmotic flow is the deflection of the constant internal electric potential lines toward the center line of the microchannel because of the change in the distribution of ions. This phenomenon leads to reconfiguration of the body force inside the bulk of the fluid. This effect can be the cause of the return flow at the entrance region of the microchannel (as shown in Fig. 4c and d) and deflection of the streamlines toward the centerline (as shown in Fig. 4b, e and f).

Fig. 5 shows the dimensionless internal electric potential distribution in the width of the microchannel at $\frac{x}{H} = 0.02$ for different amounts of κ and ΔT. This figure shows that increasing the ΔT from 0.0 to 0.75, for the same values of κ and E_x, leads to lower values of internal electric potential in central regions of the microchannel.

According to the analytical solution of the internal electric potential (Eq. (36a)), ψ is a function of κ. Moreover, according to Eq. (2), when we keep $n_{i\infty k}$ constant, λ and consequently κ may vary with the mean electrolyte temperature as ($\lambda = K^{-1} = \sqrt{\frac{\varepsilon_0 \varepsilon_r K_B T_{mean}(x)}{2Z^2 e^2 n_{i\infty}}}$). It is to say that, when there are a fixed

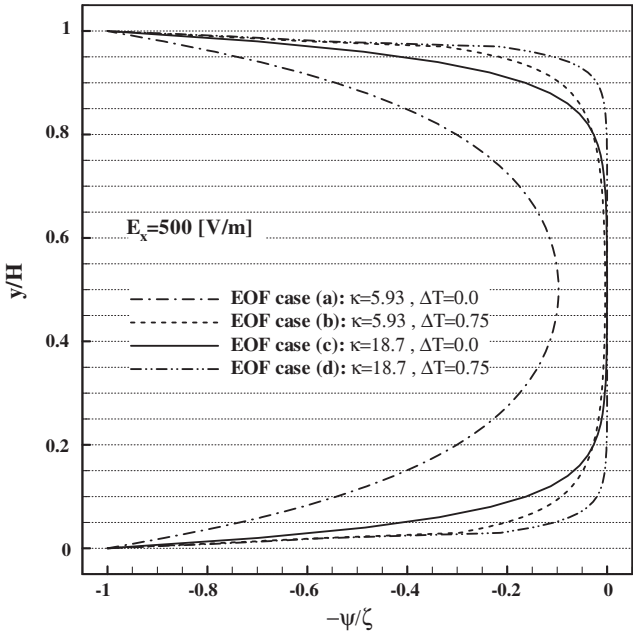

Fig. 5. Dimensionless internal electric potential distribution in the width of the channel for selected cross section $\frac{x}{H} = 0.02$. Properties of the EOFs are denoted on the figure.

number of ions in the electrolyte, it is possible to vary the thickness of the EDL by changing the temperature of the electrolyte. Therefore, we can conclude that ψ is a function of temperature. For instance, if the temperature of the electrolyte increases (assuming other parameters constant), the magnitude of the internal electric potential increases and vise versa ($\lambda \propto \sqrt{T_{mean}}$, $T_{mean} \uparrow \rightarrow \lambda \uparrow$). Therefore, at the beginning of the channel, where the fluid temperature is not raised by the wall temperature and the mean temperature is small, the amount of the internal electric potential, particularly near the center line of the microchannel, is smaller than the downstream where the electrolyte temperature is increased due to wall temperature. As shown in Fig. 5, considering the identical ion concentration (the same κ), increasing the entering electrolyte temperature difference with wall temperature (from case (a) to case (b) or from case (c) to case (d)) leads to lower internal electric potential in central regions.

Fig. 6 shows the dimensionless internal electric potential distribution along the length of microchannel for selected longitudinal sections. First, we consider the curves related to $\Delta T = 0.75$. As seen in Fig. 6, at the beginning of the microchannel for the regions near the wall, $\frac{\partial \psi}{\partial x}$ has high values. Moving from the walls toward the centerline of the microchannel, $\frac{\partial \psi}{\partial x}$ decreases. It is observed that, as seen in Fig. 4, for regions far enough from the beginning of the microchannel, $\frac{\partial \psi}{\partial x} = 0$. It is worth adding that Fig. 2a indicates that for $\Delta T = 0.0$, we have analytical solution for internal electric potential field and the LBM results are in good agreement with analytical solutions. Therefore, for $\Delta T \neq 0.0$, this is expected when the fluid moving along the microchannel and the fluid temperature approaches to the microchannel wall temperature, or in other words $T_{mean}(x) \cong T_{wall}$, consequently $\Delta T \cong 0.0$ and as a result $(\frac{\psi}{\zeta})_{LBM} \cong (\frac{\psi}{\zeta})_{Analytical\ solution}$. This is an interesting fact that Fig. 6 shows for selected amounts of longitudinal cross sections.

Fig. 7 shows the values of $\bar{\rho}_e$ on selected cross sections. Dimensionless net electric charge density is defined as $\bar{\rho}_e = \frac{\rho_e}{Zen_{i\infty}}$. The properties of the EOF are denoted on the figure. The figure shows that in the presence of temperature difference, for $\Delta T = 0.75$, near the walls, the net electric charge density at the beginning of the microchannel has higher values than the downstream of the EOF. Conversely, for the case $\Delta T = 0.0$, the net electric charge density distribution along the width of microchannel is identical for all values of $\frac{x}{H}$.

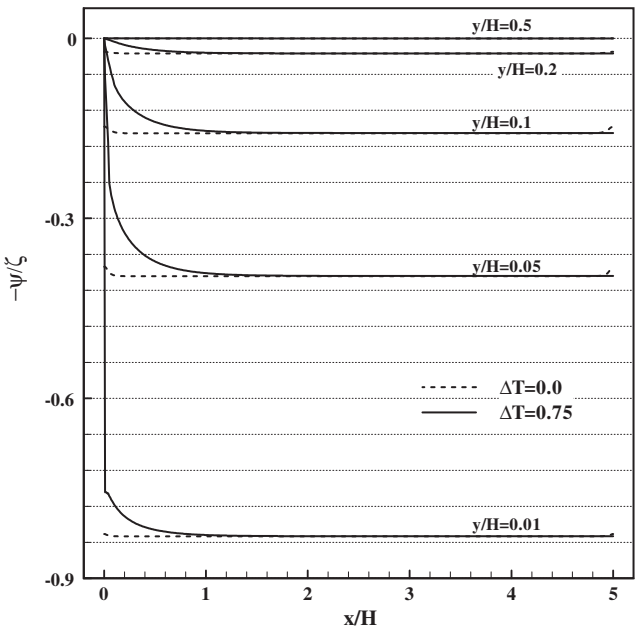

Fig. 6. Dimensionless internal electric potential distribution along the microchannel for selected longitudinal cross sections. $E_x = 500$ V/m, $\kappa = 18.7$.

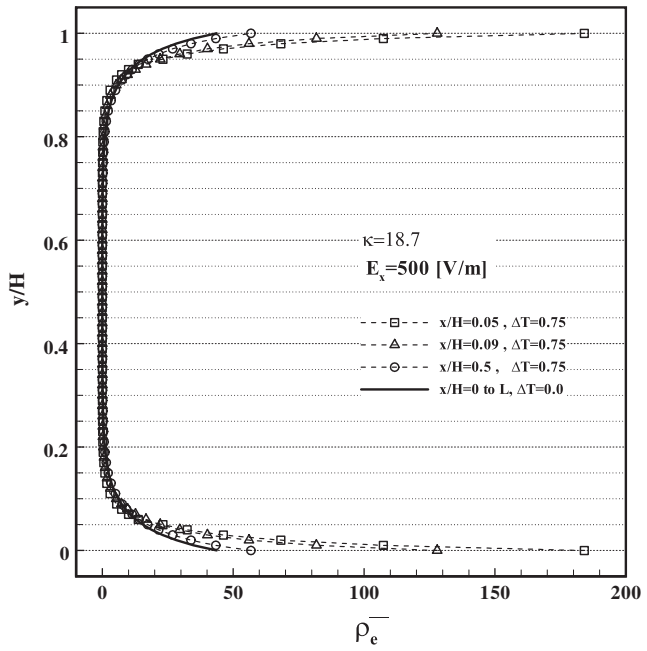

Fig. 7. Net electric charge density on selected cross sections. Properties of the EOF are denoted on the figure, $\bar{\rho}_e = \frac{\rho_e}{Zen_{i\infty}}$.

Now, regarding to descriptions those mentioned for Figs. 5–7, one can demonstrated the mechanism of vortices formation and streamline inclinations toward the centerline of the microchannel at the presence of temperature difference as follows.

Our previous discussions indicated that $\frac{\partial \psi}{\partial x}$ and net electric charge density are functions of temperature. At the same time, according to Eq. (12), electric body force is a direct function of the net electric charge density and $\frac{\partial \psi}{\partial x}$. Therefore, at the entrance of the channel, according to the results presented in Figs. 6 and 7, $\frac{\partial \psi}{\partial x}$ and net electric charge density are greater in comparison with the isothermal scenario ($\Delta T = 0.0$). In other words, when an EOF is in the presence of temperature difference, the difference between electrical body force near the walls and the central region of the microchannel is greater than the state of $\Delta T = 0.0$. It is predicted that the variation of the electric body force in this manner leads to reverse pressure gradient (increasing pressure) at the entrance region of the microchannel. Besides, as the temperature difference between the walls and electrolyte decreases along the channel ($\Delta T \rightarrow 0$), electric body force distribution becomes more uniform at the width of the microchannel. Therefore, the pressure gradient along the microchannel is predicted as a uniform decreasing pressure.

Fig. 8 evidently shows the above predictions about the pressure gradient manner in the microchannel. This figure shows the pressure distribution at selected cross sections of the microchannel for $\Delta T = 0.75$. As seen in this figure, moving from the wall toward the centerline on transverse direction, pressure increases and reaches a peak near the wall and then decreases to a nearly uniform value far away from the wall.

Near the entrance (for $\frac{x}{h} = 0.05$, 0.09 and 0.13 in the figure), for $0.2 < \frac{y}{h} < 0.8$, pressure increases in the direction of the main flow. Consequently, the return flow shown in Fig. 4c and d are justified. It should also be noted that, far away from the entrance (for example at $\frac{x}{h} = 0.5$ in the figure), the pressure distribution along the

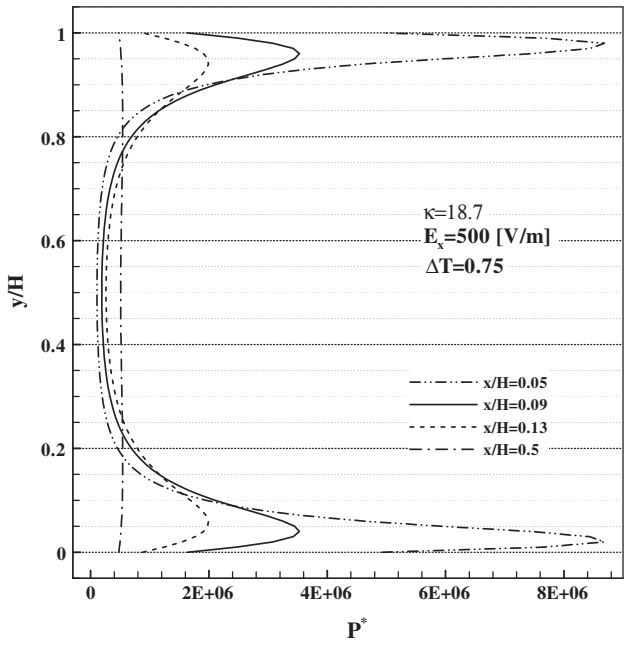

Fig. 8. Dimensionless pressure distribution in the width of the channel for selected cross sections. Properties of the flow are the same as Fig. 4d and are denoted on the figure. $P^* = \frac{P-P_{atm}}{\rho \times U_{ref}^2}$.

width of the channel becomes much more uniform. Further increase in the electric body force at the entrance and near the walls of the microchannel intensifies the higher reverse pressure gradient and therefore broadens part of the entering flow falls into the vortices flow pattern (Fig. 4c). By increasing the strength of the external electric field (E_x), the electric body force in whole width of the microchannel is increased. As a result, the distribution of electric body force in the width becomes more uniform. Therefore, the vortices flow pattern disappears, while the streamlines are inclined toward the centerline of the microchannel.

6. Conclusions

In the present paper, the temperature effects on the ions distribution have been investigated using the lattice Boltzmann method. By assuming a mean temperature across the channel, one can obtain the electric potential distribution by the Poisson–Boltzmann equation. We solve for the velocity field by incorporating the electric body force into the Navier–Stokes equations. Clearly, the Navier–Stokes, Poisson–Boltzmann, and energy equations are coupled by the temperature.

Modeling results show that by decreasing the external electric potential, decreasing the inlet electrolyte temperature relative to the wall temperature and decreasing the electric double layer thickness, at the entrance of the microchannel, a back-flow pattern (two symmetrical vortices) is formed which is available for active control of the internal flow. The vortex scale could be controlled by the strength of the external electric field and the temperature difference. This is the main significant advantage of this phenomenon for active control of the EOF without extra efforts. This pattern weakens by increasing the external electric field or decreasing the amount of temperature difference between the walls and the inlet fluid.

References

[1] S. Kandlikar, S. Garimella, D. Li, S. Colin, M.R. King, Heat Transfer and Fluid Flow in Minichannels and Microchannels, Elsevier, Amsterdam, 2006.
[2] H.A. Stone, A.D. Stroock, A. Ajdari, A. Annu, Ann. Rev. Fluid Mech. 36 (2004) 381–411.
[3] M. Wang, A. Revil, J. Colloid Interface Sci. 343 (2010) 381–386.
[4] J.C. Giddings, Sep. Sci. 1 (1966) 123–125.
[5] N.A. Polson, M.A. Hayes, Anal. Chem. 72 (2000) 1088–1092.
[6] H.H. Bau, J. Zhong, M. Yi, Sens. Actuators, B 79 (2001) 207.
[7] J.K. Wang, M. Wang, Z.X. Li, Mod. Phys. Lett. 19 (2005) 1515–1518.
[8] S.A. Mirbozorgi, H. Niazmand, M. Renksizbulut, J. Fluid Eng. 128 (2006) 1133.
[9] A.E. Herr, J.I. Molho, J.G. Santiago, M.G. Mungal, T.W. Kenny, M.G. Garguilo, Anal. Chem. 72 (2000) 1053.
[10] R.B.M. Schasfoort, S. Schlautmann, J. Hendrikse, A. Van den Berg, Science 286 (1999) 942.
[11] G. Mohiuddin Mala, D. Li, J.D. Dale, Int. J. Heat Mass Transfer 47 (2004) 987.
[12] H.S. Kwak, H. Kim, J.M. Hyun, T.-H. Song, J. Colloid Interface Sci. 335 (2009) 123.
[13] T.S. Zhao, Q. Liao, J. Micromech. Microeng. 12 (2002) 962.
[14] Q.S. Pu, S.R. Liu, Anal. Chim. Acta 511 (2004) 105–112.
[15] M.Z. Bazant, T.M. Squires, Phys. Rev. Lett. 92 (2004) 066101.
[16] T.M. Squires, M.Z. Bazant, J. Fluid Mech. 509 (2004) 217–252.
[17] J.K. Wang, M. Wang, Z.X. Li, J. Colloid Interface Sci. 296 (2006) 729.
[18] Z. Chai, B. Shi, Phys. Lett. A 364 (2007) 183.
[19] Y. Shi, T.S. Zhao, Z. Guo, Int. J. Heat Mass Transfer 51 (2008) 586.
[20] M. Wang, Q.J. Kang, J. Comput. Phys. 229 (2010) 728–744.
[21] M. Wang, S.Y. Chen, Commun. Comput. Phys. 3 (2008) 1087–1099.
[22] J.K. Wang, M. Wang, Z.X. Li, Int. J. Therm. Sci. 46 (2007) 228–234.
[23] J.H. Masliyah, Electrokinetic and Colloid Transport Phenomena, Wiley, 2006.
[24] S.A. Mirbozorgi, H. Niazmand, M. Renksizbulut, J. Fluid Eng. 129 (2007) 1346.
[25] M.C. Sukop, D.T. Throne, Lattice Boltzmann Modeling and introduction for Geoscientist and Engineers, Springer, 2007.
[26] Q. Zou, X. He, J. Phys. Fluids 9 (1997) 1591.
[27] C.H. Liu, K.H. Lin, H.C. Mai, C.A. Lin, Comput. Math. Appl. 59 (2010) 2178.
[28] W.M. Kays, M.E.Crawford, Convective Heat and Mass Transfer, 2004, Mc Graw Hill.